Reactivity of Copper in Molten Polytelluride Salts. $K_4Cu_8Te_{11}$, $A_3Cu_8Te_{10}$ (A = Rb, Cs), $AA'_2Cu_8Te_{10}$ (A, A' = K, Rb, Cs), and $A_2BaCu_8Te_{10}$ (A = K, Rb, Cs): Novel Solids Based on Endohedrally Occupied [Cu_8Te_{12}] Dodecahedral Cage-Clusters

Xiang Zhang,[†] Younbong Park,[†] Tim Hogan,[‡] Jon L. Schindler,[‡] Carl R. Kannewurf,[‡] Seeyearl Seong,[§] Thomas Albright,[§] and Mercouri G. Kanatzidis*,[†]

Contribution from the Department of Chemistry and Center for Fundamental Materials Research, Michigan State University, East Lansing, Michigan 48824, Department of Electrical Engineering and Computer Science, Northwestern University, Evanston, Illinois 60208, and Department of Chemistry and the Center for Superconductivity, University of Houston, Houston, Texas 77214-5641

Received May 26, 1995[⊗]

Abstract: The reaction of copper with molten alkali polytelluride salts led to several novel compounds with a characteristic structural feature based on a pentagonal dodecahedral geometric solid. We report here in detail the synthesis, structure, and chemical, spectroscopic, and charge-transport properties of $K_4Cu_8Te_{11}$, $A_3Cu_8Te_{10}$, and $A_2BaCu_8Te_{10}$ along with electronic band structure calculations on the two-dimensional Cu_8Te_{10} framework. $K_4Cu_8Te_{11}$ is monoclinic $C2/m$ with a = 24.086(3) Å, b = 6.821(6) Å, c = 18.461(3) Å, β = 124.45(1)°, V = 2501 Å^3 at 23 °C, Z = 4, no. of data used ($I > 3\sigma(I)$) 2029, no. of variables 121. The final R/R_w was 2.5%/3.7%. $Rb_3Cu_8Te_{10}$ is monoclinic $C2/m$ with a = 24.420(11) Å, b = 6.974(6) Å, c = 6.933(1) Å, β = 104.90(1)°, V = 1141 Å^3 at 23 °C, Z = 2, no. of data used ($I > 3\sigma(I)$) 721, no. of variables, 57 final R/R_w 5.7%/7.3%. $Cs_3Cu_8Te_{10}$ is orthorhombic $Immm$ with a = 7.053(2) Å, b = 24.159(3) Å, c = 6.935(3) Å, V = 1182 Å^3 at 23 °C, Z = 2, no. of data used ($I > 3\sigma(I)$) 839, no. of variables 36 final R/R_w 3.2%/5.0%. $K_{0.9}Cs_{2.1}Cu_8Te_{10}$ is orthorhombic $Immm$ with a = 7.023(3) Å, b = 23.895(6) Å, c = 6.908(3) Å, V = 1159 Å^3 at 23 °C, Z = 2 no. of data used ($I > 3\sigma(I)$) 625, no. of variables 37, final R/R_w 3.5%/3.0%. $K_2BaCu_8Te_{10}$ is monoclinic $C2/m$ with a = 23.245(5) Å, b = 6.950(5) Å, c = 7.061(5) Å, β = 101.23(4)°, V = 1119 Å^3 at 23 °C, Z = 2, no. of data used ($I > 3\sigma(I)$) 1445, no. of variables 57, final R/R_w 8.8%/11.3%. $Cs_2BaCu_8Te_{10}$ is orthorhombic $Immm$ with a = 7.109(2) Å, b = 23.761(16) Å, c = 6.966(3) Å, V = 1177 Å^3 and Z = 2, no. of data used ($I > 3\sigma(I)$) 795, no. of variables 35, final R/R_w 3.0%/6.0%. All compounds reported here, except $K_4Cu_8Te_{11}$, contain the same layered Cu/Te framework built from the [Cu_8Te_{12}] pentagonal dodecahedral cage-cluster. This characteristic cluster, however, is also the building block of the three-dimensional structure of $K_4Cu_8Te_{11}$. The structure consists of condensed pentagonal dodecahedral $Cu_8(Te_2)_6$ clusters sharing Te−Te edges. Each $Cu_8(Te_2)_6$ dodecahedral cluster encapsulates an alkali or a Ba^{2+} ion. The $A_3Cu_8Te_{10}$ are mixed valence compounds and exhibit metallic properties as demonstrated by electrical conductivity, thermoelectric power, and magnetic susceptibility measurements. $K_4Cu_8Te_{11}$ and $A_2BaCu_8Te_{10}$ are electron-precise semiconductors with narrow band gaps. Extended-Hückel theoretical tight binding calculations on $A_3Cu_8Te_{10}$ confirm the metallic nature of the materials.

Introduction

The pace of studying transition and main-group metal tellurides has accelerated in the last decade even though it is still playing a catch-up role compared to that of the lighter chalcogen analogs.[1,2] We have been interested in exploring the synthetic chemistry of new solid-state copper tellurides from the now-established polychalcogenide flux method, particularly at intermediate temperatures.[3−5] Recently, we reported in preliminary communication the ternary copper−polytelluride compounds $K_4Cu_8Te_{11}$ and $K_2Cu_5Te_5$ as products of the reaction of Cu with molten K_2Te_x at 350 °C.[6] $K_4Cu_8Te_{11}$[6a] was found to contain a three-dimensional network with a unique Cu_8Te_{12} cage-cluster encapsulating a K^+ ion, while $K_2Cu_5Te_5$[6b,c] repre-

[⊗] Abstract published in *Advance ACS Abstracts*, October 1, 1995.

(1) (a) Draganjac, D.; Rauchfuss, T. B. *Angew. Chem., Int. Ed. Engl.* **1985**, *24*, 742−757. (b) Müller, A. *Polyhedron* **1986**, *5*, 323−340. (c) Müller, A.; Diemann, E. *Adv. Inorg. Chem.* **1987**, *31*, 89−122. (d) Kanatzidis, M. G. *Comments Inorg. Chem.* **1990**, *10*, 161−195. (e) Ansari, M. A.; Ibers, J. A. *Coord. Chem. Rev.* **1990**, *100*, 223−266. (f) Roof, L. C.; Kolis, J. W. *Chem. Rev.* **1993**, *93*, 1037−1080. (g) Kanatzidis, M. G.; Huang, S.-P. *Coord. Chem. Rev.* **1994**, *130*, 509−621.

(2) (a) Jobic, S.; Deniard, P.; Brec, R.; Rouxel, J.; Jouanneaux, A.; Fitch, A. N. *Z. Anorg. Allg. Chem.* **1991**, *598/599*, 199−215. (b) Canadell, E.; Jobic, S.; Brec, R.; Rouxel, J. *J. Solid State Chem.* **1992**, *99*, 189−199. (c) Canadell, E.; Monconduit, L.; Evain, M.; Brec, R.; Rouxel, J.; Wangbo, M.-H. *Inorg. Chem.* **1993**, *32*, 10−12.

(3) (a) Kanatzidis, M. G. *Chem. Mater.* **1990**, *2*, 353−363. (b) Kanatzidis, M. G.; Park, Y. *J. Am. Chem. Soc.* **1989**, *111*, 3767−3769. (c) McCarthy, T.; Zhang, X.; Kanatzidis, M. G. *Inorg. Chem.* **1993**, *32*, 2944−2948. (d) Liao, J.-H.; Varotsis, C.; Kanatzidis, M. G. *Inorg. Chem.* **1993**, *32*, 2453−2462. (e) McCarthy, T. J.; Ngeyi, S.-P.; Liao, J.-H.; DeGroot, D. C.; Hogan, T.; Kannewurf, C. R.; Kanatzidis, M. G. *Chem. Mater.* **1993**, *5*, 331−340.

(4) (a) Dhingra, S.; Kanatzidis, M. G. *Science* **1992**, *258*, 1769−1772. (b) Park, Y.; Kanatzidis, M. G. *Angew. Chem., Int. Ed. Engl.* **1990**, *29*, 914−915. (c) Sutorik, A. C.; Kanatzidis, M. G. *J. Am. Chem. Soc.* **1991**, *113*, 7754−7755.

(5) (a) Zhang, X.; Kanatzidis, M. G. *J. Am. Chem. Soc.* **1994**, *116*, 1890−1898. (b) Zhang, X.; Kanatzidis, M. G. *Inorg. Chem.* **1994**, *33*, 1238−1240. (c) Zhang, X.; Kanatzidis, M. G. Manuscript in preparation.

(6) (a) Park, Y.; DeGroot, D. C.; Schindler, J.; Kannewurf, C. R.; Kanatzidis, M. G. *Angew. Chem., Int. Ed. Engl.* **1991**, *30*, 1325−1328. (b) Park, Y.; Kanatzidis, M. G. *Chem. Mater.* **1991**, *3*, 781−783. (c) Seong, S.; Albright, T.; Zhang, X.; Kanatzidis, M. G. *J. Am. Chem. Soc.* **1994**, *116*, 7287−7293.

0002-7863/95/1517-10300$09.00/0

sents an intermediate structure between that of CuTe[7] and NaCuTe.[8] Since the Cu_8Te_{12} cage does not have a S or Se analog and it forms with an encapsulated K^+, we investigated whether it could be stabilized in the presence of other counterions. We examined the effect of fluxes with larger alkali ions A_2Te_x (A = Rb, Cs) as well as mixed alkali $A_{2-2x}A'_xTe_y$ (A, A′ = K, Rb, Cs) and $A_{2-2x}Ba_xTe_y$ fluxes. In the mixed Ba-rich polytelluride $A_{2-2x}Ba_xTe_y$ (A = Na, K) systems, the reaction of Cu produced $NaBa_6Cu_{3-\delta}Te_{14}$ and the X-ray isomorphous $(K_{0.60}Ba_{0.40})Ba_6Cu_{2.58}Te_{14}$, two new quaternary polytelluride compounds of a novel structure type.[9a] These copper-deficient phases contain discrete $[Cu_3Te_3(Te_3)_3]^{9-}$ clusters arranged in columnar stacks along the *c*-axis via intercluster Te···Te contacts. Our continuing studies of Cu reactivity led to a new class of solid-state Cu/Te compounds, which possess a different structure from $K_4Cu_8Te_{11}$ but also contain the Cu_8Te_{12} cluster. These compounds are new additions to the relatively limited number of solid-state copper polytellurides known so far in the literature, which include CuTe, $K_2Cu_5Te_5$, $K_4Cu_8Te_{11}$, $NaBa_6Cu_{3-\delta}Te_{14}$, and $(Me_4N)CuTe_4$.[10] In addition to these, other related phases in the A/Cu/Te system are $NaCu_3Te_2$,[11a] KCu_3Te_2,[11b] NaCuTe,[8] and KCuTe,[8a] all of which contain monotelluride ions. We report here in detail the synthesis, structure, chemical, spectroscopic, and charge-transport properties of $K_4Cu_8Te_{11}$, $A_3Cu_8Te_{10}$, and $A_2BaCu_8Te_{10}$ along with electronic tight-binding calculations on the two-dimensional Cu_8Te_{10} framework.

Experimental Section

Reagents. Chemicals in this work were used as obtained: (i) copper electrolytic dust, Fisher Scientific Co., Fairlawn, NJ; (ii) barium telluride powder (20 mesh), Cerac Inc., Milwaukee, WI; (iii) tellurium powder (200 mesh), rubidium metal (analytical reagent), cesium metal (analytical reagent), Johnson Matthey/AESAR Group, Seabrook, NH; (iv) potassium metal (analytical reagent), Mallinckrodt Inc., Paris, KY; (v) dimethylformamide (DMF) (analytical reagent), diethyl ether (ACS anhydrous), EM Science, Inc., Gibbstown, NJ.

Alkali metal chalcogenides K_2Te, Rb_2Te, and Cs_2Te were prepared in liquid ammonia from alkali metals and elemental tellurium as described earlier.[12]

Synthesis. All manipulations were carried out in a glovebox under a nitrogen atmosphere. All yields reported are based on Cu.

$K_4Cu_8Te_{11}$ (1). Amounts of 0.064 g (1.0 mmol) of Cu, 0.309 g (1.5 mmol) of K_2Te and 0.765 g (6.0 mmol) of Te were mixed and loaded in a Pyrex tube and flame-sealed under vacuum ($\sim 10^{-4}$ Torr). The tube was placed in a computer-controlled furnace and heated at 350 °C for 3 days and cooled slowly at 2 °C/h to 100 °C. Black needle-like crystals, sometimes with a small contamination of elemental tellurium, were obtained after the excess K_2Te_x flux was removed by washing with DMF under nitrogen gas atmosphere. Yield was 57%. A semiquantitative microprobe analysis performed on a large number of single crystals with energy dispersive spectroscopy (EDS) under a scanning electron microscope (SEM) gave an average composition of $K_{4.0}Cu_{8.3}Te_{10.8}$.

$Rb_3Cu_8Te_{10}$ (2). Amounts of 0.032 g (0.50 mmol) of Cu, 0.299 g (1.00 mmol) of Rb_2Te, and 0.510 g (4.00 mmol) of Te were mixed and loaded in a Pyrex tube and flame-sealed under vacuum. The tube was placed in a computer-controlled furnace and heated at 350 °C for 4 days and cooled slowly at 2 °C/h to 50 °C. Black chunky crystals were obtained as majority of product contaminated with a small amount of elemental tellurium, after the excess Rb_2Te_x flux was removed by washing with DMF under nitrogen atmosphere. Yield was 55%. A semiquantitative microprobe analysis performed on a large number of single crystals gave an average composition of $Rb_{3.0}Cu_{8.1}Te_{9.9}$.

$Cs_3Cu_8Te_{10}$ (3). Amounts of 0.032 g (0.5 mmol) of Cu, 0.197 g (0.5 mmol) of Cs_2Te, and 0.383 g (3.0 mmol) of Te were used as above. The tube was heated at 450 °C for 4 days and cooled slowly to 100 °C at a rate of 2 °C/h and then to 50 °C at a rate of 10 °C/h. A small amount of black, platelike crystals was obtained as a minor phase along with a large amount of powder containing elemental tellurium and Cs_2Te_x flux. The matrix, a hard mass, does not dissolve easily in DMF, water, or any other common organic solvent. Thus, we have crushed the matrix to manually isolate single crystals. Semiquantitative microprobe analysis performed on a large number of single crystals gave an average composition of $Cs_{3.0}Cu_{7.8}Te_{9.9}$.

$KRb_2Cu_8Te_{10}$ (4). Amounts of 0.032 g (0.50 mmol) of Cu, 0.103 g (0.50 mmol) of K_2Te, 0.075 g (0.25 mmol) of Rb_2Te, and 0.383 g (3.00 mmol) of Te were used. The tube was heated at 360 °C for 6 days and cooled slowly at 2 °C/h to 50 °C. Black chunky crystals were obtained contaminated with a small amount of elemental Te. Yield was 62%. Semiquantitative microprobe analysis performed on a large number of single crystals gave an average composition of $K_{1.0}Rb_{1.7}Cu_{8.0}Te_{9.7}$.

$K_{0.9}Cs_{2.1}Cu_8Te_{10}$ (5). Amounts of 0.032 g (0.50 mmol) of Cu, 0.103 g (0.50 mmol) of K_2Te, 0.099 g (0.25 mmol) of Cs_2Te, and 0.383 g (3.00 mmol) of Te were used. The tube was heated at 420 °C for 4 days and cooled slowly at 2 °C/h to 100 °C. Black chunky crystals were obtained contaminated with a small amount of elemental Te. Yield was 54%. Semiquantitative microprobe analysis performed on a large number of single crystals gave an average composition of $K_{0.9}Cs_{1.4}Cu_{8.0}Te_{9.7}$.

$K_2BaCu_8Te_{10}$ (6). Amounts of 0.032 g (0.50 mmol) of Cu, 0.206 g (1.00 mmol) of K_2Te, 0.066 g (0.25 mmol) of BaTe, and 0.383 g (3.00 mmol) of Te were used. The tube was heated at 370 °C for 4 days and cooled slowly at 2 °C/h to 100 °C. Black chunky crystals were obtained as a majority product contaminated with a small amount of elemental Te and BaTe. Yield was 80%. A semiquantitative microprobe analysis performed on a large number of single crystals system gave an average composition of $K_{1.7}Ba_{0.9}Cu_{8.0}Te_{10.0}$.

$Rb_2BaCu_8Te_{10}$ (7). Amounts of 0.032 g (0.50 mmol) of Cu, 0.149 g (0.50 mmol) of Rb_2Te, 0.066 g (0.25 mmol) of BaTe and 0.255 g (2.00 mmol) of Te were used. The tube was heated at 480 °C for 4 days and cooled at 2 °C/h to 200 °C and then at 5 °C/h to 100 °C. Large black chunky crystals were obtained with a yield of 85%. Semiquantitative microprobe analysis performed on a large number of single crystals gave an average composition of $Rb_{2.0}Ba_{1.0}Cu_{8.0}Te_{9.7}$.

$Cs_2BaCu_8Te_{10}$ (8). Amounts of 0.032 g (0.50 mmol) of Cu, 0.393 g (1.00 mmol) of Cs_2Te, 0.132 g (1.00 mmol) of BaTe, and 0.383 g (3.00 mmol) of Te were used. The tube was heated at 420 °C for 4 days and cooled slowly at 2 °C/h to 100 °C. Mostly black chunky crystals were obtained contaminated with some elemental Te, BaTe, and excess Cs_2Te_x despite prolonged washing with DMF. Yield was 50%. Microprobe analysis performed on a large number of single crystals gave an average composition of $Cs_{1.8}Ba_{1.2}Cu_{8.0}Te_{9.5}$.

Physical Measurements. Electron Microscopy. Semiquantitative microprobe analysis of the compounds was performed with a JEOL JSM-35C scanning electron microscope (SEM) equipped with a Tracor Northern energy dispersive spectroscopy (EDS) detector. Data were acquired using an accelerating voltage of 20 kV and a 30-s accumulation time. Standardless analysis was performed. The results reported are an average of multiple measurements done on several single crystals of a given compound.

Thermal Analysis. Differential thermal analysis (DTA) was performed on a computer-controlled Shimadzu DTA-50 thermal analyzer. Typically a sample (~15 mg) of ground crystalline material was sealed in quartz ampules under vacuum. A quartz ampule of equal mass filled with Al_2O_3 was sealed and placed on the reference side of the detector. The sample was heated to the desired temperature at 10 °C/min, then isothermed for 10 min and finally cooled down to 100

(7) (a) Patzak, I. *Z. Metallkd.* **1956**, *47*, 418–420. (b) Baranova, R. V.; Pinsker, Z. G. *Kristallografiya* **1964**, *9*, 83–85. (c) Anderko, K.; Schubert, K. *Z. Metallkd.* **1954**, *45*, 371–378.

(8) (a) Savelsberg, G.; Schäfer, H. *Z. Naturforsch.* **1978**, *33b*, 370–373. (b) Park, Y. Ph.D. Dissertation, Michigan State University, 1992.

(9) (a) Zhang, X.; Schindler, J. L.; Hogan, T.; Kannewurf, C. R.; Kanatzidis, M. G. *Angew. Chem., Int. Ed. Engl.* **1995**, 34, 68–71. (b) Zhang, X.; Kanatzidis, M. G. Unpublished results.

(10) Kim, K.; Kanatzidis, M. G. *J. Am. Chem. Soc.* **1993**, *115*, 5871–5872.

(11) (a) Savelsberg, G.; Schäfer, H. *Mater. Res. Bull.* **1981**, *16*, 1291–1297. (b) Klepp, K. O. *J. Less-Common Met.* **1987**, *128*, 79–89

(12) (a) Klemm, W.; Sodomann, H.; Langmesser, P. *Z. Anorg. Allg. Chem.*, **1939**, *241*, 281–304. (b) Feher, F. In *Handbuch der Praparativen Anorganischen Chemie*; Brauer, G., Ed.; Ferdinand Enke: Stuttgart, Germany, 1954; pp 280–281.

°C at the same rate. The residue of the DTA experiment was examined by X-ray powder diffraction.

Charge-Transport Measurements. DC electrical conductivity and thermopower measurements were made on single crystals and polycrystalline compactions of the compounds. Conductivity measurements were performed in the usual four-probe geometry with 60- and 25-mm diameter gold wires used for the current and voltage electrodes, respectively. Measurements of the sample cross-sectional area and voltage probe separation were made with a calibrated binocular microscope. Conductivity data were obtained with the computer-automated system described elsewhere.[13a] Thermoelectric power measurements were made by using a slow AC technique[13b] with 60-μm gold wires used to support and conduct heat to the sample, as well as to measure the voltage across the sample resulting from the applied temperature gradient. In both measurements, the gold electrodes were held in place on the sample with a conductive gold paste. Mounted samples were placed under vacuum (10^{-3} Torr) and heated to 320 K for 2−4 h to cure the gold contacts. For a variable-temperature run, data (conductivity or thermopower) were acquired during sample warming. The average temperature drift rate during an experiment was kept below 0.3 K/min. Multiple variable-temperature runs were carried out for each sample to ensure reproducibility and stability. At a given temperature, reproducibility was within ±5%.

Magnetic Susceptibility Measurements. Magnetic susceptibility measurements were carried out on a MPMS Quantum Design SQUID magnetometer. Measurements were made on single crystals and polycrystalline materials. Field dependence measurements were always performed first, and a suitable magnetic field was chosen from the linear region for temperature-dependence measurements. The data were corrected for the diamagnetism of the constituent elements and of the sample container.

Crystallographic Studies. All compounds were examined by X-ray powder diffraction for the purpose of phase purity and identification. Accurate d_{hkl} spacings (Å) were obtained from the powder patterns recorded on a calibrated (with FeOCl as internal standard) Phillips XRG-3000 computer-controlled powder diffractometer with Ni-filtered Cu Kα radiation operating at 35 kV and 35 mA. They were found to match the patterns calculated on the basis of atomic positions found from the single crystal structure analyses.[14]

Structure Solution of $K_4Cu_8Te_{11}$. A crystal with dimensions 0.60 × 0.06 × 0.06 mm was put on the end of a glass fiber and mounted on a Rigaku AFC6S four-circle automated diffractometer equipped with a graphite-crystal monochromator. A C-centered monoclinic cell was determined from indexing a list of autosearched reflections with 4° < 2θ < 20°. Intensity data were collected using the ω−2θ scan mode. The stability of the crystal was monitored by measuring three standard reflections periodically (every 150 reflections) during the course of data collection. No crystal decay was detected for this compound and all the others. The space group was chosen on the basis of systematic absences and intensity statistics. The structure was solved by direct methods using SHELXS-86[15a] and refined by full-matrix least-squares techniques of the TEXSAN package of crystallographic programs.[15b] An empirical absorption correction based on ψ scans was applied to the data, followed by a DIFABS correction to the isotropically refined data.[15c] All atoms were eventually refined anisotropically. The final atomic coordinates and equivalent isotropic temperature factors are given in Table 1.

Structure Solution of $Rb_3Cu_8Te_{10}$. A crystal with dimensions 0.20 × 0.03 × 0.02 mm was put on the end of a glass fiber and mounted on a Rigaku AFC6S four-circle automated diffractometer. A C-centered monoclinic cell was determined from indexing a list of autosearched reflections with 4° < 2θ < 20°. Intensity data were collected using the ω−2θ scan mode. The space group was chosen on the basis of systematic absences and intensity statistics. The structure was solved by direct methods using SHELXS-86 and refined by full-matrix least-squares techniques of the TEXSAN package of crystallographic programs. An empirical absorption correction based on ψ scans was applied to the data, followed by a DIFABS correction to the isotropically refined data. All atoms were eventually refined anisotropically. The final atomic coordinates and equivalent isotropic temperature factors are given in Table 2.

Table 1. Positional Parameters and B(eq) for $K_4Cu_8Te_{11}$

atom	x	y	z	B(eq)
Te(1)	0.037 55(4)	0	0.130 04(5)	1.12(3)
Te(2)	0.090 26(4)	0	0.310 31(5)	1.14(3)
Te(3)	−0.065 44(4)	−1/2	−0.018 54(5)	1.14(3)
Te(4)	−0.094 55(3)	−0.295 01(9)	0.181 19(3)	1.36(2)
Te(5)	0.071 21(4)	−1/2	0.441 96(5)	1.45(3)
Te(6)	0.197 40(4)	−1/2	0.467 92(5)	1.19(3)
Te(7)	0.228 61(3)	0.294 96(9)	0.274 74(4)	1.44(2)
Te(8)	−0.042 66(4)	0	0.407 21(5)	1.47(3)
Te(9)	−0.188 48(4)	0	-0.057 65(5)	1.30(3)
Cu(1)	0.007 40(5)	−0.206 0(2)	0.336 73(7)	1.81(4)
Cu(2)	0.204 63(6)	0.192 4(2)	0.387 66(7)	1.90(4)
Cu(3)	−0.079 33(6)	−0.193 9(2)	0.058 21(7)	1.68(4)
Cu(4)	0.128 86(5)	−0.193 2(2)	0.118 57(7)	1.65(4)
K(1)	0.064 0(1)	−1/2	0.222 2(2)	1.9(1)
K(2)	−0.127 4(2)	1/2	0.329 9(2)	2.7(1)
K(3)	0.354 1(1)	1/2	0.474 3(2)	2.1(1)
K(4)	−0.249 9	0	0.086 7(2)	3.8(2)

Table 2. Positional Parameters and B(eq) for $Rb_3Cu_8Te_{10}$ and $Cs_3Cu_8Te_{10}$

atom	x	y	z	B(eq)
		$Rb_3Cu_8Te_{10}$		
Te(1)	−0.0594(1)	−1/2	0.4462(4)	1.1(1)
Te(2)	0.0001(1)	0	0.2040(4)	1.1(1)
Te(3)	−0.1480(1)	−0.3004(3)	−0.1367(3)	1.53(8)
Te(4)	0.1684(1)	0	0.6559(5)	1.4(1)
Rb(1)	0.2233(3)	1/2	0.714(1)	3.8(3)
Rb(2)	0	−1/2	0	1.5(2)
Cu(1)	0.0936(2)	−0.1936(5)	0.3912(6)	1.7(2)
Cu(2)	−0.0936(2)	−0.1940(5)	0.2179(6)	1.7(1)
		$Cs_3Cu_8Te_{10}$		
Cs(1)	1/2	0.22267(6)	1.0000	2.98(6)
Cs(2)	1/2	0	1/2	0.98(5)
Te(1)	1/2	0.05808(4)	1.0000	0.99(4)
Te(2)	1.0000	0	0.2962(1)	1.02(4)
Te(3)	0.3026(1)	0.14514(3)	1/2	1.37(3)
Te(4)	1.0000	0.16360(5)	1.0000	1.27(4)
Cu	0.1946(2)	0.09123(5)	1.1958(1)	1.62(4)

Structure Solution of $Cs_3Cu_8Te_{10}$. A crystal with dimensions 0.39 × 0.18 × 0.08 mm was mounted on a glass fiber. Intensity data for the crystal were collected using the ω−2θ scan mode on a Rigaku AFC6S four-circle automated diffractometer. An I-centered orthorhombic cell was determined from indexing of a list of autosearched reflections. The structure was best solved in space group *Immm* by direct methods using SHELXS-86 and refined by full-matrix least-squares techniques of the TEXSAN package of crystallographic programs. Absorption corrections were applied as above. All atoms were eventually refined anisotropically. The final atomic coordinates and equivalent isotropic temperature factors are given in Table 2.

Cell Determination of $KRb_2Cu_8Te_{10}$. The quality of the crystals was generally low and most were twinned. Only the unit cell was determined, which was obtained from indexing of a partial list of autosearched reflections. The cell parameters are a = 24.33(3) Å, b = 6.961(6) Å, c = 6.926(6) Å, β = 104.79(8)°, and V = 1134(2) Å^3. This C-centered monoclinic cell is very similar to that of the isomorphous $Rb_3Cu_8Te_{10}$.

Structure Solution of $K_{0.9}Cs_{2.1}Cu_8Te_{10}$. A crystal with dimensions of 0.36 × 0.36 × 0.28 mm was mounted on a glass fiber. The data collection was performed on a Nicolet Autodiffractometer (Siemens). The orthorhombic cell obtained from indexing of a list of autosearched reflections is very similar to that of $Cs_3Cu_8Te_{10}$. The structure was solved with direct methods using SHELXS-86 and refined with the TEXSAN programs. Absorption corrections were applied as above. As with all $A_3Cu_8Te_{10}$ structures, there are two crystallographically

(13) (a) Lyding, J. W.; Marcy, H. O.; Marks, T. J.; Kannewurf, C. R. *IEEE Trans. Instrum. Meas.* **1988**, *37*, 76−80. (b) Marcy, H. O.; Marks, T. J.; Kannewurf, C. R. *IEEE Trans. Instrum. Meas.* **1990**, *39*, 756−760.

(14) CERIUS Version 3.1, Molecular Simulations, 1992.

(15) (a) Sheldrick, G. M. In *Crystallographic Computing 3*; Sheldrick, G. M., Kruger, C., Doddard, R., Eds.; Oxford University Press: Oxford, England, 1985; pp 175−189. (b) *TEXSAN: Singel Crystal Structure Analysis Software*, Version 5.0; Molecular Structure Corp.: The Woodlands, Texas. (c) Walker, N.; Stuart, D. *Acta Crystallogr.* **1983**, *39A*, 158−166.

Table 3. Crystal Data and Experimental Details for $K_4Cu_8Te_{11}$, $Rb_3Cu_8Te_{10}$, $Cs_3Cu_8Te_{10}$, $K_{0.9}Cs_{2.1}Cu_8Te_{10}$, $K_2BaCu_8Te_{10}$, and $Cs_2BaCu_8Te_{10}$

	$K_4Cu_8Te_{11}$	$Rb_3Cu_8Te_{10}$	$Cs_3Cu_8Te_{10}$	$K_{0.9}Cs_{2.1}Cu_8Te_{10}$	$K_2BaCu_8Te_{10}$	$Cs_2BaCu_8Te_{10}$
weight	2068.36	2040.73	2183.08	2098.65	1999.88	2187.50
crystal size, mm	0.60 × 0.06 × 0.06	0.20 × 0.03 × 0.02	0.39 × 0.18 × 0.08	0.36 × 0.36 × 0.28	0.40 × 0.15 × 0.10	0.60 × 0.25 × 0.10
crystal system	monoclinic	monoclinic	orthorhombic	orthorhombic	monoclinic	orthorhombic
a, Å	24.086(3)	24.420(11)	7.053(2)	7.023(3)	23.245(5)	7.109(2)
b, Å	6.821(6)	6.974(6)	24.159(3)	23.895(8)	6.950(5)	23.761(16)
c, Å	18.461(3)	6.933(10)	6.935(3)	6.908(3)	7.061(5)	6.966(3)
β, deg	124.45(1)	104.87(89)			101.23(4)	
V, Å^3	2501(3)	1141(3)	1182(1)	1159(1)	1119(1)	1177(2)
space group	*C2/m* (no. 12)	*C2/m* (no. 12)	*Immm* (no. 71)	*Immm* (no. 71)	*C2/m* (no. 12)	*Immm* (no. 71)
Z	4	2	2	2	2	2
d_{calcd}, g/cm^3	5.49	5.94	6.14	6.02	5.94	6.17
λ(Mo Kα), Å	0.71069	0.71069	0.71069	0.71073	0.71069	0.71069
μ, cm^{-1}	199.8	206.8	237.4	229.9	223.9	239.7
temp, °C	23	23	23	23	23	23
$2\theta_{max}$, deg	50	50	60	55	60	50
octants	$0 \rightarrow h,k,-l \rightarrow l$	$0 \rightarrow h,k,-l \rightarrow l$	$0 \rightarrow hkl$	$0 \rightarrow hkl$	$0 \rightarrow h,k,-l \rightarrow l$	$0 \rightarrow hkl$
scan type	$\omega-2\theta$	$\omega-2\theta$	$\omega-2\theta$	$\omega-2\theta$	$\omega-2\theta$	$\omega-2\theta$
extinction coeff	3.50×10^{-7}	1.03×10^{-7}	2.05×10^{-7}	1.12×10^{-7}	0.28×10^{-7}	N/A
no. of reflns colld	2535	1129	1014	819	3577	658
no. of unique reflns	2480	1102	1014	789	3504	634
no. of reflns obsd ($F_o^2 > 3\sigma(F_o^2)$)	2029	721	839	625	1445	570
no. of variables	121	57	36	37	57	35
R, Rw[a]	0.025, 0.037	0.057, 0.073	0.032, 0.050	0.035, 0.030	0.088, 0.113	0.030, 0.060
goodness of fit	1.64	2.49	2.26	2.62	4.80	2.87
max peak, e/Å^3	1.63	2.46	1.97	2.65	9.78	2.39
min peak, e/Å^3	−1.66	−2.72	−1.45	−3.37	−7.50	−1.72

[a] $R = \sum||F_o| - |F_c||/\sum|F_o|$. $R_w = [\sum w(|F_o| - |F_c|)^2/\sum w|F_o|^2]^{1/2}$.

distinct positions for the alkali cations. One of them is occupied exclusively by Cs^+ ions. The other position appears to be filled by K^+ ions, but refinement of the structure with exclusive occupation of this position by K^+ gave a negative B_{eq} value for K. This site was best modeled by mixed occupancy of K^+ and Cs^+ ions. The refinement of the populations resulted in partial occupancy (89% by K and 11% by Cs) giving the reported formula.

Structure Solution of $K_2BaCu_8Te_{10}$. A crystal with dimensions of 0.45 × 0.15 × 0.10 mm was mounted on a glass fiber. The quality of the crystals was low as they also tend to grow twinned. Nevertheless, a crystal was found from which a reasonable data set could be obtained. The intensity data were collected on a Rigaku AFC6S diffractometer. The unit cell is C-centered monoclinic, similar to that of $Rb_3Cu_8Te_{10}$. The structure was refined with the TEXSAN programs. Absorption corrections were applied as above. The final residuals of the refinement were large, even after the (200) reflection (which had a $\Delta F/\sigma F > 100$) was removed from the calculations. The refinement results are thought to be reliable, since the standard deviations of the bond distances and angles are acceptable, and the temperature factors of all atoms are comparable to those of the other isostructural compounds.

Cell Determination of $Rb_2BaCu_8Te_{10}$. This compound is isomorphous to $Rb_3Cu_8Te_{10}$. The quality of the crystals was again low, and only the unit cell was determined. The cell parameters are a = 23.93(4) Å, b = 7.015(4) Å, c = 6.974(10) Å, β = 105.8(1)°, and V = 1137(3) Å^3.

Structure Solution of $Cs_2BaCu_8Te_{10}$. A crystal with dimensions of 0.60 × 0.25 × 0.10 mm was mounted on a glass fiber. Intensity data were collected on a Rigaku AFC6S diffractometer. The compound is isomorphous to $Cs_3Cu_8Te_{10}$. The structure was solved with direct methods and refined with TEXSAN programs. Absorption corrections were applied as above.

All calculations were performed on a VAXstation 3100 Model 76 computer. The complete data collection parameters, details of the structure solution and refinement for all compounds are given in Table 3.

Computational Methods. Tight binding calculations with an extended Hückel-Hamiltonian[16] using a modified Wolfsberg–Helmholz formula[17] have been used for the calculations. The atomic parameters have been obtained from previous work.[18,19] The geometrical details were taken from the experimental structure of $Cs_3Cu_8Te_{10}$. The Cs atoms were neglected in the calculation. A 64K point set was used for the two-dimensional calculations of one $Cu_8Te_{10}^{3-}$ layer.

Results and Discussion

Structures. All compounds reported here, except $K_4Cu_8Te_{11}$, contain the same layered Cu/Te framework built from the $[Cu_8Te_{12}]$ pentagonal dodecahedral cage-cluster. This characteristic cluster, however, is also the building block of the three-dimensional structure of $K_4Cu_8Te_{11}$. We will describe the structure of $K_4Cu_8Te_{11}$ before illustrating how the new structures are built and then discuss the effect of the alkali/alkaline earth ions on the dodecahedral cluster and the overall Cu/Te framework.

Structure of $K_4Cu_8Te_{11}$. The three-dimensional structure of $K_4Cu_8Te_{11}$ (**1**) is shown in Figure 1. It has a Cu/Te framework with large tunnels running parallel to the b axis which are filled with K^+ ions. This complicated framework can be tailored from fused and linked recognizable $[Cu_8Te_{12}]$ (or $Cu_8(Te_2)_6$) clusters. One such pentagonal dodecahedral $Cu_8(Te_2)_6$ cluster cage is shown in Figure 2. This geometric platonic solid (ideal point group T_h) is made of fused planar Cu_2Te_3 pentagons each with a ditelluride edge. A remarkable feature of this dodecahedral cage is the encapsulation of a K^+ ion in its center. Each cage-cluster contains three mutually perpendicular sets of ditelluride units. One of these sets is shared with adjacent $[Cu_8Te_{12}]$ clusters to form a linear cage column, and two such columns share one ditelluride of another set to form a wider double cage-column. In addition, these double cage-columns running along the b axis are capped by monotellurides and assemble side by side through intercolumn Cu–Te bonding interactions to form a corrugated Cu/Te layer parallel to the (2,0,−1) plane. Two perpendicular views of this layer are given in Figure 3. The Te atoms participating in the intercolumn Cu–Te interactions belong to the unshared ditelluride of the second

(16) (a) Hoffmann, R. *J. Chem. Phys.* **1963**, *39*, 1397. (b) Hoffmann, R.; Lipscomb, W. N. *ibid.* **1962**, *36*, 2197. (c) Whangbo, M.-H.; Hoffmann, R.; Woodward, R. B. *Proc. R. Soc. London, Ser. A* **1979**, *366*, 23.

(17) Ammeter, J. H.; Burgi, H.-B.; Thiebeault, J. C.; Hoffmann, R. *J. Am. Chem. Soc.* **1978**, *100*, 3686.

(18) Hay, P. J.; Thibeault, J. C.; Hoffmann, R. *J. Am. Chem. Soc.* **1975**, *97*, 4884.

(19) Hughbanks, T. Private communication.

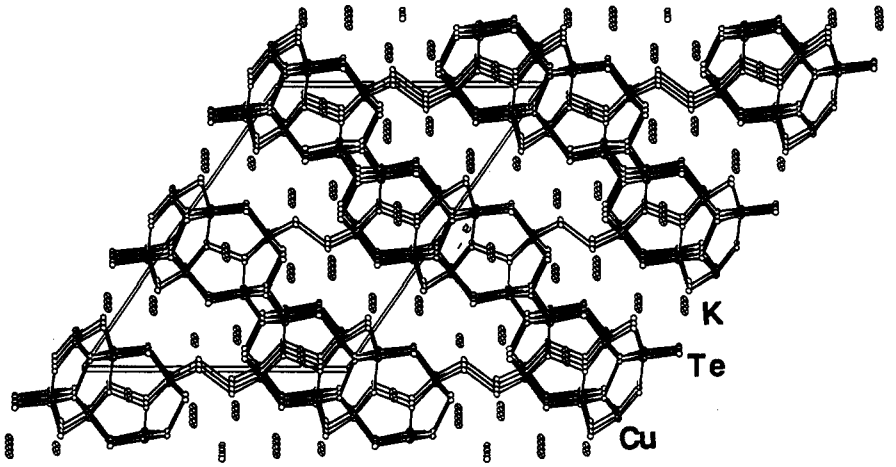

Figure 1. ORTEP presentation of the three-dimensional structure of $K_4Cu_8Te_{11}$.

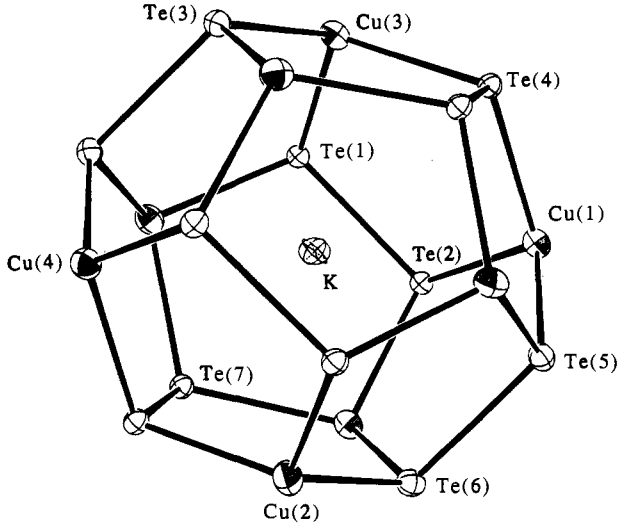

Figure 2. Structure of the K^+-filled Cu_8Te_{12} cage-cluster in $K_4Cu_8Te_{11}$.

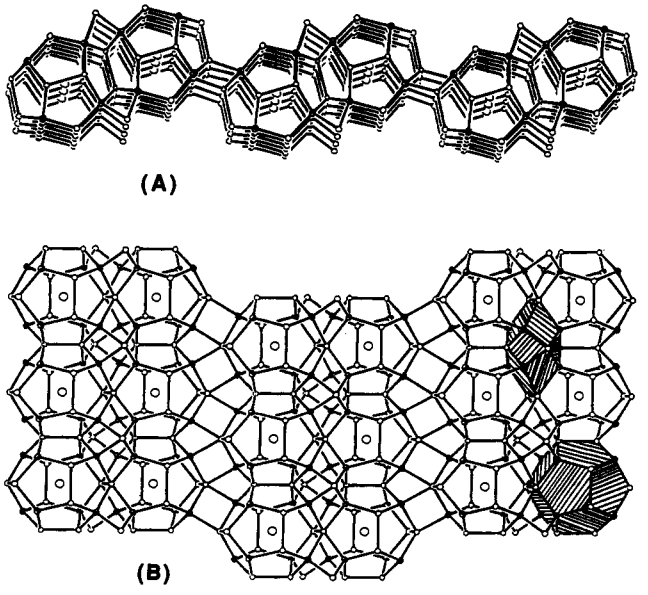

Figure 3. One two-dimensional fragment cut from the three-dimensional $K_4Cu_8Te_{11}$ showing the assembling from the Cu_8Te_{12} clusters.

set. The third set of ditelluride units is unshared. The Cu/Te layers are then connected to each other through bridging ditellurides, resulting in large channels as shown in Figure 1. The coordination geometry around the Cu atoms is distorted

Table 4. Selected Cu–Te Distances (Å) and Te–Cu–Te Angles (deg) in $K_4Cu_8Te_{11}$

Cu(1)–Te(2)	2.701(2)	Cu(3)–Te(1)	2.685(2)
Cu(1)–Te(4)	2.582(1)	Cu(3)–Te(3)	2.649(2)
Cu(1)–Te(5)	2.604(2)	Cu(3)–Te(4)	2.590(1)
Cu(1)–Te(8)	2.626(2)	Cu(3)–Te(9)	2.622(1)
Cu(2)–Te(2)	2.627(2)	Cu(4)–Te(1)	2.673(2)
Cu(2)–Te(6)	2.631(2)	Cu(4)–Te(3)	2.633(2)
Cu(2)–Te(6)	2.699(1)	Cu(4)–Te(7)	2.594(1)
Cu(2)–Te(7)	2.556(1)	Cu(4)–Te(9)	2.625(1)
Te(2)–Cu(1)–Te(4)	104.86(4)	Te(1)–Cu(3)–Te(3)	103.78(5)
Te(2)–Cu(1)–Te(5)	110.54(5)	Te(1)–Cu(3)–Te(4)	109.09(4)
Te(2)–Cu(1)–Te(8)	113.85(6)	Te(1)–Cu(3)–Te(9)	116.22(6)
Te(4)–Cu(1)–Te(5)	115.92(6)	Te(3)–Cu(3)–Te(4)	112.47(6)
Te(4)–Cu(1)–Te(8)	105.22(5)	Te(3)–Cu(3)–Te(9)	109.45(5)
Te(5)–Cu(1)–Te(8)	106.56(5)	Te(4)–Cu(3)–Te(9)	106.00(5)
Te(2)–Cu(2)–Te(6)	110.86(6)	Te(1)–Cu(4)–Te(3)	105.69(5)
Te(2)–Cu(2)–Te(6)	108.76(5)	Te(1)–Cu(4)–Te(7)	109.28(4)
Te(2)–Cu(2)–Te(7)	110.17(5)	Te(1)–Cu(4)–Te(9)	117.42(6)
Te(6)–Cu(2)–Te(6)	97.52(5)	Te(3)–Cu(4)–Te(7)	111.82(6)
Te(6)–Cu(2)–Te(7)	117.66(5)	Te(3)–Cu(4)–Te(9)	109.85(5)
Te(6)–Cu(2)–Te(7)	111.02(6)	Te(7)–Cu(4)–Te(9)	102.91(5)

tetrahedral. The average Cu–Te bond distance of the monotellurides is 2.624(2) Å. The bond distances between Cu and Te_2^{2-} ligands range from 2.556(1) to 2.701(2) Å with an average Cu–Te distance of 2.63(4) Å. The Te–Te distances of the ditellurides are in the range 2.796(1)~2.828(2) Å with an average of 2.81(1) Å. The shortest intertelluride distance is indicative of nonbonding at 4.0 Å. Selected bond distances and angles are given in Table 4.

There are four crystallographically distinct K^+ ions in this structure. The encapsulated K(1) atom, sitting on a mirror plane perpendicular to the *b* axis, is surrounded by the 12 Te atoms of the cage. K–Te distances range from 3.676(3) to 3.960(3) Å with an average of 3.75(8) Å. The remaining three K atoms are located in the tunnels with average K–Te distances of 3.70(16) Å for K(2), 3.66(23) Å for K(3), and 3.71(9) Å for K(4).

Structures of $Rb_3Cu_8Te_{10}$ and $Cs_3Cu_8Te_{10}$. The new structure type of $Rb_3Cu_8Te_{10}$ (**2**) contains $[RbCu_8Te_{10}]_n^{2n-}$ layers separated by layers of Rb^+ cations. It crystallizes in a monoclinic cell as shown in Figure 4A. Despite the significant structural difference from **1**, the building block of this structure is also the cagelike Cu_8Te_{12} pentagonal dodecahedron. However, this dodecahedron now encapsulates a Rb^+ ion, which sits on a mirror plane perpendicular to the *b* axis, see Figure 5. The Cu_8Te_{12} clusters form layers parallel to the (100) plane by sharing two pairs of oppositely spaced ditellurides (i.e., $Te(1)_2^{2-}$ and $Te(2)_2^{2-}$) along the *b* and *c* axis, respectively, see Figure 6. The third type of $Te(3)_2^{2-}$ units is unshared and lines the

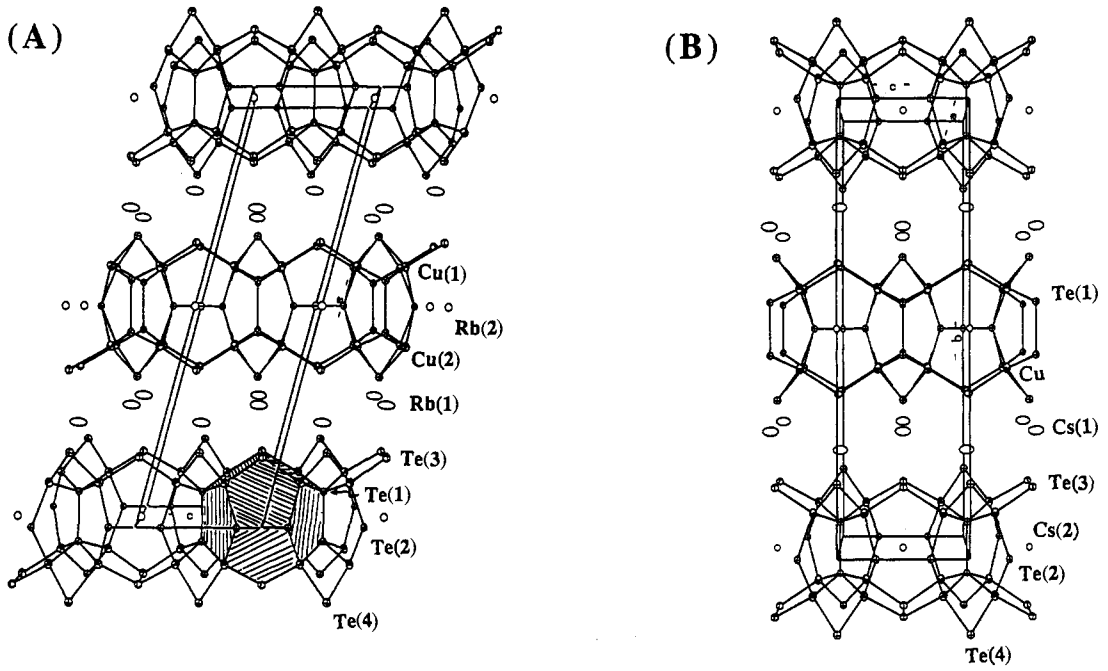

Figure 4. (A) Packing diagram of $Rb_3Cu_8Te_{10}$. (B) Unit cell of $Cs_3Cu_8Te_{10}$.

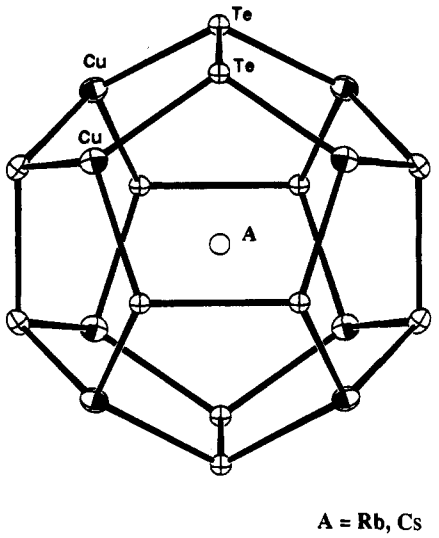

Figure 5. Structure of the $[ACu_8Te_{12}]$ cage-cluster (A = Rb, Cs) in $A_3Cu_8Te_{10}$.

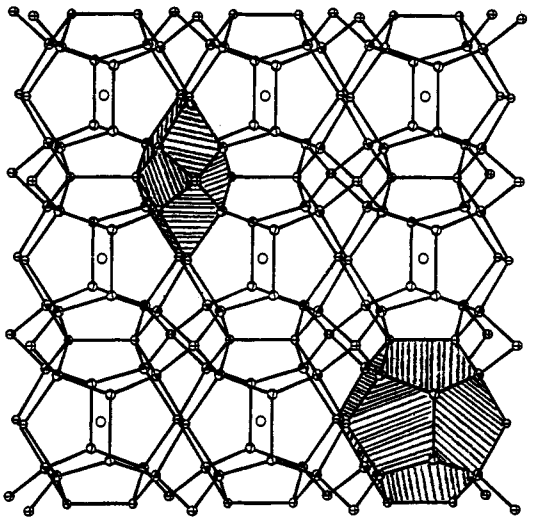

Figure 6. One $[RbCu_8Te_{10}]_n^{2n-}$ layer assembled from fusion of $Cu_8(Te_2)_6$ clusters through sharing of two perpendicular sets of ditellurides.

surface of the Cu_8Te_{10} layers. There are two crystallographically independent Cu atoms in the structure. The Cu atoms are bonded to three Te atoms (which belong to three Te_2^{2-} units) inside the layer. In addition, they are capped by quadruply bonded μ_4-Te^{2-} ions above and below the layer. The geometry around the Cu atom is slightly distorted tetrahedral. The average Cu−Te bond distance of the monotellurides (e.g., $Te(4)^{2-}$) is 2.604(5) Å, which is slightly shorter than that found in **1**. The bond distances between Cu and Te_2^{2-} ligands range from 2.576(5) to 2.684(5) Å with an average of 2.64(5) Å. The Te−Te distances of the three ditellurides are in the range 2.784(4)~2.828(4) Å with an average of 2.80(2) Å. The shortest distance is the Te(3)−Te(3) at 2.784(4) Å. These distances are similar to others reported in the literature and are also very close to those found in **1**. The Cu−Te bond distances associated with the unshared ditelluride set (i.e., $Te(3)_2^{2-}$) are shorter by 0.1 Å than other Cu−Te distances. The shortest nonbonding intertelluride distance is also nonbonding at 4.1 Å.

Among the two types of Rb^+ cations in the structure, there are twice as many located between the Cu_8Te_{10} layers as in the center of dodecahedral $Cu_8(Te_2)_6$ cluster. The $Rb(1)^+$ ions are seven coordinate with Rb−Te distances ranging from 3.698(6) to 4.190(9) Å. The endohedral $Rb(2)^+$ ions are surrounded by the 12 Te atoms of the $Cu_8(Te_2)_6$ cage with Rb−Te distances in the narrow range 3.738(5)−3.763(3) Å. On the basis of these data one could expect that $Rb(1)^+$ ions have larger thermal motions than $Rb(2)^+$ ions, as it is indeed observed.

The structure of $Cs_3Cu_8Te_{10}$ (**3**) is similar to that of **2** but it crystallizes in the orthorhombic system as shown in Figure 4B. The higher symmetry brings some minor structural modifications. All Cu atoms become equivalent. The dodecahedral Cu_8Te_{12} cluster has a crystallographic D_{2h} symmetry, and the endohedral $Cs(2)^+$ now sits on three mutually perpendicular mirror planes. Otherwise the structure is essentially same as described above. The Cu−Te distance and Te−Te distance of ditellurides are very close to those found in **2**. Again the cations sitting between the layers have a large anisotropic temperature factor compared to that of the other more confined cations, which is the general case for all structures reported here.

Structures of Quaternary Phases and Ion Selectivity of the $[Cu_8Te_{12}]$ Cage. This unique, covalently bonded cluster framework structure was previously unknown in solid-state compounds, although the pentagonal dodecahedral motif has

Table 5. Selected Te−Te and Cu−Te Distances (Å) and Te−Cu−Te Angles (deg)

	$Rb_3Cu_8Te_{10}$[a]	$Cs_3Cu_8Te_{10}$	$KCs_2Cu_8Te_{10}$	$K_2BaCu_8Te_{10}$[a]	$Cs_2BaCu_8Te_{10}$
Te(1)−Te(1)	2.802(4)	2.806(2)	2.786(3)	2.805(4)	2.796(3)
Te(2)−Te(2)	2.828(4)	2.826(2)	2.817(3)	2.856(5)	2.849(3)
Te(3)−Te(3)	2.784(4)	2.785(2)	2.777(3)	2.765(4)	2.765(2)
Cu−Te(1)	2.655(6)	2.670(1)	2.654(2)	2.665(2)	2.688(2)
Cu−Te(2)	2.682(2)	2.688(1)	2.668(2)	2.684(7)	2.680(2)
Cu−Te(3)	2.580(6)	2.594(1)	2.577(2)	2.578(4)	2.572(2)
Cu−Te(4)	2.604(6)	2.605(1)	2.605(2)	2.607(2)	2.607(2)
Te(1)−Cu−Te(2)	106.7(1)	107.33(5)	107.63(6)	106.9(7)	107.86(7)
Te(1)−Cu−Te(3)	109.7(4)	109.10(5)	109.01(7)	109.6(4)	107.32(6)
Te(1)−Cu−Te(4)	111.0(2)	111.18(5)	111.22(6)	110.2(2)	111.59(6)
Te(2)−Cu−Te(3)	110.0(3)	110.54(5)	110.08(7)	107.3(6)	108.42(6)
Te(2)−Cu−Te(4)	115.6(3)	114.62(5)	114.81(7)	116.5(1)	115.01(6)
Te(3)−Cu−Te(4)	103.8(2)	103.99(5)	103.99(6)	106(2)	106.33(7)

[a] Averaged values for Cu(1) and Cu(2).

been seen in the organic compounds of the dodecahedrane $C_{20}H_{20}$ and its derivatives.[20] If we ignore the alkali metal content of the cage, the Cu_8Te_{12} fragment is topologically equivalent to the structure initially proposed for M_8C_{12} (M = Ti, V, Zr, Hf), the metal carbide species which have been recently identified by gas phase studies.[21] Given the different electronic structures of Cu_8Te_{12} and M_8C_{12}, it is difficult to assess whether they share a common origin for their stability. Indeed, more recent theoretical findings[22] have suggested very different structures for the M_8C_{12} clusters that are dominated by M−M bonding. That Cu_8Te_{12} is filled with an alkali ion suggests that a templating mechanism might be responsible for forming the cluster. To probe this point further we decided to determine if the ionic size of the "template" or ionic charge is more important in cage formation. We also wondered whether, given a choice, the Cu_8Te_{12} cage could display any cation selectivity. Thus, we employed mixed-alkali fluxes and mixed alkali-alkaline earth fluxes. Synthetic explorations with Na_2Te_x did not yield compounds with Cu_8Te_{12} cages.

The K/Cs mixed compound $KCs_2Cu_8Te_{10}$ (**5**) is isomorphous to **3** and crystallizes in the orthorhombic system. The Cu/Te framework and the Cu−Te and Te−Te distances are little changed compared to those of $Cs_3Cu_8Te_{10}$. From the occupancy refinement it was found that Cs^+ ions sit between the layers, *while the center of the [Cu_8Te_{12}] cage is occupied mostly by K^+ ions*. Due to the poor crystal quality we could not obtain a complete single crystal analysis of the K/Rb mixed compound **4**, which is isomorphous to the monoclinic **2**. Elemental analysis of the products from mixed fluxes with various K/Rb ratios indicates a formula of $K_{1-x}Rb_{2+x}Cu_8Te_{10}$, where x appears to increase slightly with increasing Rb in the flux. The amount of Rb in this compound was found to be at least twice as much as that of K even from K-rich fluxes. The 2:1 ratio of Rb:K may suggest that Rb^+ occupies the sites between the layers, and thus the dodecahedral cage prefers the smaller K^+.

$K_2BaCu_8Te_{10}$ (**6**) and $Rb_2BaCu_8Te_{10}$ (**7**) are X-ray isomorphous to **2**. From the single crystal structure analysis of **6** it was found that the center of the [Cu_8Te_{12}] cage is occupied by the Ba^{2+} ion while the K^+ ion sits between the layers. In the orthorhombic structure of $Cs_2BaCu_8Te_{10}$ (**8**), which is isomorphous to **3**, the cage is also occupied by the Ba^{2+} ion. Overall, the cage appears to have a higher affinity for cations with high charge/radius ratios, given that the radius of the cation is not too small. This preference is probably electrostatic in origin as the anionic layers of $[Cu_8Te_{10}]^{n-}$ strive to reduce their negative charge. The $A_3Cu_8Te_{10}$ are formally mixed-valent compounds (see discussion below). The introduction of Ba into the structure produces the electron-precise $A_2BaCu_8Te_{10}$.

The crystal symmetry seems to depend on the size of the ions occupying the interlayer space, reflecting differences in packing of these cations. The large Cs^+ ion results in an orthorhombic lattice while the smaller ions (e.g., K^+, Rb^+) choose a monoclinic lattice. This is a general case for both ternary and quaternary phases reported here. Despite some minor differences, the Cu_8Te_{10} frameworks display metric data similar to each other. For comparison, the most important Cu−Te and Te−Te bond distances and angles of all five compounds are listed in Table 5.

Comparison of $Cu_8(Te_2)_6$ Cages. The presence of the same structural building unit $Cu_8(Te_2)_6$ in the three-dimensional $K_4Cu_8Te_{11}$ and the two-dimensional $A_3Cu_8Te_{10}/A_2BaCu_8Te_{10}$ phases here attests to its significant stability. Selected metric data for the dodecahedral cages are given in Table 6. If we consider the interactions between the encapsulated ions and tellurium atoms as ionic, the average A−Te distance is ca. 3.75 Å in all compounds. These similar distances lead to almost negligible change in the volumes of the dodecahedral cages. Calculation of the entire volume of each cluster indicated a ~5 $Å^3$ decrease in going from [$CsCu_8Te_{12}$] to [KCu_8Te_{12}] and a ~4 $Å^3$ decrease from [$CsCu_8Te_{12}$] to [$BaCu_8Te_{12}$]. However, these volume changes are still small compared to the changes in volumes from Cs^+ to K^+ (11 $Å^3$) and to Ba^{2+} (12 $Å^3$). Careful examination of the cage dimensions (defined as the distances between each mutually parallel ditelluride set) in [$BaCu_8Te_{12}$] further reveals that, relative to the cage dimensions involving the alkali ions, the Cu_8Te_{12} cluster is slightly compressed along the axis perpendicular to the $[BaCu_8Te_{10}]^{2-}$ layers. This reduces the symmetry of the pentagonal dodecahedron from the ideal T_h to D_{2h}. The distance between the unshared opposite ditellurides is 0.16−0.35 Å shorter than those associated with the shared ditellurides. The distortion of the cage effected by Ba^{2+} is explained by the fact that the unshared ditellurides are more negatively charged than the shared ones thus subject to stronger Coulombic attraction to the more positively charged encapsulated ion. This suggests that the Cu_8Te_{12} cage is rigid along the layer dimensions but somewhat elastic perpendicular to them.

Synthesis. The synthesis of $K_4Cu_8Te_{11}$, $Rb_3Cu_8Te_{10}$, and $Cs_3Cu_8Te_{10}$ has been accomplished by using polytelluride fluxes as solvents and reagents according to the unbalanced eqs 1−3:

(20) Ternansky, R. J.; Balogh, D. W.; Paquette, L. A. *J. Am. Chem. Soc.* **1982**, *104*, 4503−4504.

(21) (a) Guo, B. C.; Kerns, K. P.; Castleman, A. W., Jr. *Science* **1992**, *255*, 1411−1413. (b) Guo, B. C.; Wei, S.; Purnell, J.; Buzza, S.; Castleman, A. W., Jr. *Science* **1992**, *256*, 515−516.

(22) (a) Lin, Z.; Hall, M. B. *J. Am. Chem. Soc.* **1993**, *115*, 11165. (b). Rohmer, M. M.; De Vaal, P.; Benard, M. *Ibid.* **1992**, *114*, 9696. Rohmer, M. M.; Benard, M.; Henriet, C.; Bo, C.; Poblet, J. M. *J. Chem. Soc., Chem. Commun.* **1993**, 1182. (c) Dance, I. *Ibid.* **1992**, 1779.

Table 6. Selected Metric Data for the $ACu_8(Te_2)_6$ Cluster

	$KCu_8(Te_2)_6$	$RbCu_8(Te_2)_6$	$CsCu_8(Te_2)_6$	$KCu_8(Te_2)_6$	$BaCu_8(Te_2)_6$	$BaCu_8(Te_2)_6$
compd	$K_4Cu_8Te_{11}$	$Rb_3Cu_8Te_{10}$	$Cs_3Cu_8Te_{10}$	$KCs_2Cu_8Te_{10}$	$K_2BaCu_8Te_{10}$	$Cs_2BaCu_8Te_{10}$
dimens, Å	6.821(6)	6.933(10)	6.935(3)	6.908(3)	6.950(5)	6.966(3)
	7.091(4)	6.974(6)	7.053(2)	7.023(3)	7.061(5)	7.109(2)
	6.955(4)	6.987(6)	7.013(2)	6.924(3)	6.794(3)	6.755(5)
$d_{av(Te-Te)}$, Å	2.81(1)	2.80(2)	2.81(2)	2.79(2)	2.81(5)	2.80(4)
$d_{max(A-Te)}$, Å	3.960(3)	3.763(3)	3.779(1)	3.784(2)	3.808(3)	3.830(1)
$d_{min(A-Te)}$, Å	3.676(3)	3.738(5)	3.741(1)	3.724(2)	3.668(2)	3.650(2)
$d_{av(A-Te)}$, Å	3.75(8)	3.75(1)	3.77(3)	3.75(3)	3.74(6)	3.74(7)
$d_{av(Cu-A)}$, Å	3.69(2)	3.73(1)	3.735(1)	3.715(2)	3.76(2)	3.762(2)
$d_{av(Cu-Te)}$, Å	2.64(4)	2.64(5)	2.65(5)	2.63(4)	2.66(4)	2.65(5)
volume, Å^3	145.9	146.5	150.8	145.2	146.5	147.3
radius of A^{n+}, Å	1.78	1.86	2.02	1.78	1.75	1.75
volume of A^{n+}, Å^3	23.6	27.0	34.5	23.6	22.4	22.4

$$2Cu + 3K_2Te + 12Te \rightarrow K_4Cu_8Te_{11} \quad (1)$$

$$Cu + 2Rb_2Te + 8Te \rightarrow Rb_3Cu_8Te_{10} \quad (2)$$

$$Cu + Cs_2Te + 6Te \rightarrow Cs_3Cu_8Te_{10} \quad (3)$$

Complete melts form at the temperatures employed (350~450 °C). $K_4Cu_8Te_{11}$ was made from the reaction of 2 mol of Cu with 3 mol of K_2Te_5 at 350 °C. The stability of this compound in the polytelluride flux is largely dependent on the flux composition and the reaction temperature. When Cu was reacted to a more basic (shorter-chained) Te_x^{2-} or at slightly higher temperature, $K_2Cu_5Te_5$ was obtained.[6b] From even more basic flux or at higher temperatures, the known monotellurides KCu_3Te_2 and KCuTe were obtained. This situation follows the general trend that lower temperature and acidic flux conditions favor polychalcogenide compounds, while higher temperature and basic conditions tend to form monochalcogenides, see reactions Scheme 1.

In the Rb/Cu/Te system the compound $Rb_3Cu_8Te_{10}$ was stabilized from a range of polytelluride fluxes in a wider temperature window of 350−450 °C. Albeit less stable, $Rb_2Cu_5Te_5$ could still be obtained from basic flux at higher temperature.[23] $Cs_3Cu_8Te_{10}$ is the only ternary compound we found from the reaction of Cu with Cs_2Te_x.

Experiments with fluxes containing two different alkali ions gave rise to mixed alkali copper tellurides with the general formula of $AA'_2Cu_8Te_{10}$ see eqs 4 and 5. No phase separation was evident.

$$Cu + K_2Te + 0.5Rb_2Te + 6Te \rightarrow KRb_2Cu_8Te_{10} + \text{flux} \quad (4)$$

$$Cu + K_2Te + 0.5Cs_2Te + 6Te \rightarrow KCs_2Cu_8Te_{10} + \text{flux} \quad (5)$$

The incorporation of two types of alkali ions with similar function in the same structural framework might naturally lead to disorder and nonstoichiometry. This occurred most in $KRb_2Cu_8Te_{10}$ and least in $KCs_2Cu_8Te_{10}$, where the size difference between K^+ and Cs^+ is the largest. In both cases we notice that the least basic K^+ ion incorporates in a lower fraction even though the reactive fluxes are K-rich. When we decreased the amount of K^+ in the mixed fluxes, we still obtained a K/Cs mixed phase close to $KCs_2Cu_8Te_{10}$, but in the case of K/Rb, the K/Rb ratio was slightly decreased with $K_{1-x}Rb_{2+x}Cu_8Te_{10}$. The preference of larger alkali counterions in these compounds may be attributed to the greater basicity of Cs and Rb.

When the Ba^{2+} cation was introduced into the polytelluride fluxes, a series of mixed alkali/alkaline earth copper tellurides

Scheme 1

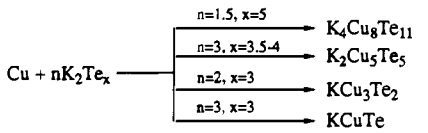

were obtained with the formula of $A_2BaCu_8Te_{10}$ as shown:

$$Cu + mA_2Te + nBa_2Te + 6Te \rightarrow A_2BaCu_8Te_{10} + \text{flux} \quad (A = K, Rb, Cs) \quad (6)$$

These Ba-containing compounds are stoichiometric and are related to $A_3Cu_8Te_{10}$ by replacement of one Ba for an alkali atom. The Ba phases are accessible from polytelluride fluxes in a wide temperature range over 350 °C and thus are more stable than their alkali analogs.

Differential thermal analysis (DTA) experiments performed on the crystalline materials indicate that the ternary alkali compounds $Rb_3Cu_8Te_{10}$ and $Cs_3Cu_8Te_{10}$ undergo decomposition when brought to melting at 390 and 361 °C, respectively. X-ray powder diffraction analysis of the residue material for the Rb compound showed decomposition to $Rb_2Cu_5Te_5$ and Te. On the contrary, the Ba-containing quaternary compounds melt congruently. For example, DTA indicates that $Rb_2BaCu_8Te_{10}$ melts at 490 °C and recrystallizes at 468 °C. The incorporation of cations with a high charge/radius ratio (e.g., Ba^{2+}) into Cu/Te frameworks points to a new avenue of synthetic exploration in this area.[9,24]

Charge Transport and Optical Properties. The formula of $K_4Cu_8Te_{11}$ can be written as $K_4[Cu_8(Te_2)_5Te]$. If the formal charges of the ditelluride and monotelluride units are considered to be −2, and that of Cu as +1, the compound is electron-precise and should be a semiconductor. This is confirmed by electrical conductivity measurements, where the value at room temperature is relatively high at 160 S/cm. The temperature dependence of the conductivity is thermally activated as would be expected of a semiconductor, see Figure 7. The other phases can be divided into two categories according to their electronic structures. The first group includes $A_3Cu_8Te_{10}$ or $AA'_2Cu_8Te_{10}$ with $[Cu_8(Te_2)_4(Te)_2]^{3-}$ frameworks, which are mixed-valent compounds: on the basis of the same assumption of −2 on each ditelluride and telluride unit, the formal oxidation states on Cu atoms are +1 (seven atoms) and +2 (one atom). However, in mixed-valence copper chalcogenide compounds, it is generally accepted that the formal oxidation state of copper is +1.[6,25,26] This is because the Cu d orbitals lie lower in energy relative to Te p orbitals (see below). This would place the one-electron hole on a tellurium p band consisting mainly of p orbitals of either the ditellurides or the monotelluride atoms.

(23) (a) $Rb_2Cu_5Te_5$ is X-ray isomorphous to $K_2Cu_5Te_5$: space group *Cmcm* (no. 63), a = 4.1610(8) Å, b = 16.418(4) Å, c = 18.677(5) Å, V = 1275.9(9) Å^3 at 23 °C, no. of reflections measured 701, no. of unique data 367, no. of unique data observed with $I > 3\sigma(I)$ 271, R = 0.027, R_w = 0.035, GOF = 1.36. (b) Zhang, X.; Kanatzidis, M. G. Unpublished results.

(24) Zhang, X.; Kanatzidis, M. G. Manuscript in prepartion.

(25) Folmer, J. C. W.; Jellinek F. *J. Less-Common Met.* **1980**, *76*, 153−162.

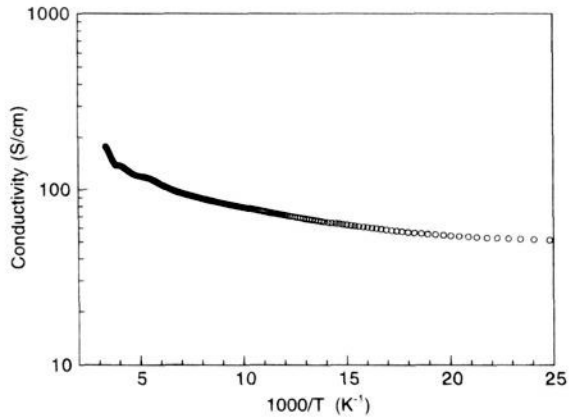

Figure 7. Single crystal variable-temperature four-probe resistivity data for $K_4Cu_8Te_{11}$.

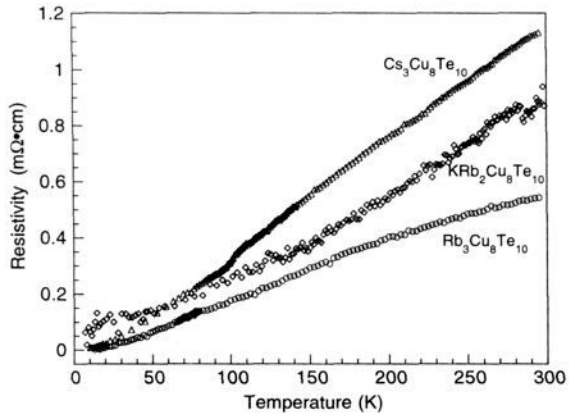

Figure 8. Variable-temperature four-probe resistivity data measured on single crystals of (A) $Rb_3Cu_8Te_{10}$, (B) $Cs_3Cu_8Te_{10}$, and (C) $KRb_2Cu_8Te_{10}$.

These materials are thus expected to be p-type metallic conductors. The second group of $A_2BaCu_8Te_{10}$ are electron-precise as replacement of Ba^{2+} for an alkali ion provides an additional electron to fill the hole in the valence band. As a result, they are expected to be semiconductors.

Charge transport measurements on single crystals of $Rb_3Cu_8Te_{10}$, $Cs_3Cu_8Te_{10}$, and $KRb_2Cu_8Te_{10}$ over the temperature range 5−300 K show that they are excellent metallic conductors. For example, the resistivity of $Cs_3Cu_8Te_{10}$ increases from 1.2×10^{-6} Ω cm at 5 K to 1.1×10^{-3} Ω cm at room temperature, see Figure 8. The resistivities of these compounds at 5 K are among the lowest known for ternary Cu chalcogenides. The temperature dependence of the thermoelectric power (Seebeck coefficient) in these materials show very small positive values of 1∼6 μV/K in the temperature range 90∼300 K as shown in Figure 9. The small and linearly increasing Seebeck coefficient with rising temperature independently confirms that $A_3Cu_8Te_{10}$ are p-type metals as suggested from the band-filling argument advanced above and from the theoretical extended-Hückel calculations.

(26) (a) Canadell, E.; Jobic, S.; Brec, R.; Rouxel, J. *J. Solid State Chem.* **1992**, *98*, 59. (b) Canadell, E.; Whangbo, M.-H. *Inorg. Chem.* **1990**, *29*, 1398. (c) Jobic, S.; Brec, R.; Rouxel, J. *J. Solid State Chem.* **1992**, *96*, 169. (d) Lee, S.; Hoistad, L. M.; Kampf, J. *New J. Chem.* **1992**, *16*, 657. (e) Mar, A.; Jobic, S.; Ibers, J. A. *J. Am. Chem. Soc.* **1992**, *114*, 8963. (f) Whangbo, M.-H.; Canadell, E. *Ibid.* **1992**, *114*, 9587. (g) Ansari, M. A.; Bollinger, J. C.; Ibers, J. A. *Ibid.* **1993**, *115*, 3838. (h) Canadell, E.; Mathey, Y.; Whangbo, M. H. *J. Am. Chem. Soc.* **1988**, *110*, 104. (i) Jobic, S.; Brec, R.; Rouxel, J. *J. Solid State Chem.* **1992**, *98*, 59. (j) Gressier, P.; Whangbo, M. H. Canadell, E. *Inorg. Chem.* **1984**, *23*, 1228. (k) Mitchell, J. F.; Burdett, J. K.; Keane, P. M.; Ibers, J. A.; Degroot, D. C.; Hogan, J. P.; Schindler, J. L.; Kannewurt, C. R. *J. Solid State Chem.* **1992**, *99*, 103.

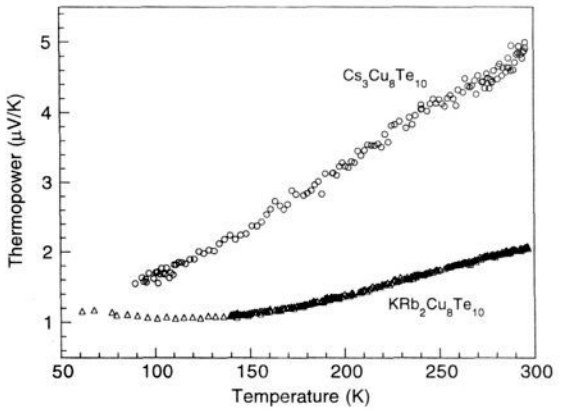

Figure 9. Variable-temperature thermoelectric power data measured on single crystals of (A) $Rb_3Cu_8Te_{10}$, (B) $Cs_3Cu_8Te_{10}$, and (C) $KRb_2Cu_8Te_{10}$.

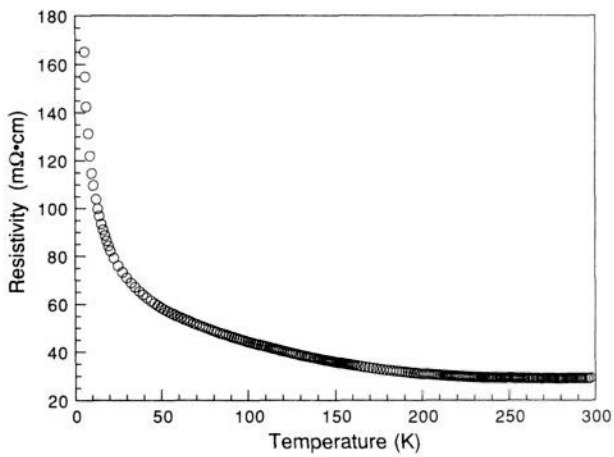

Figure 10. Variable-temperature four-probe resistivity data measured on a single crystals of $Rb_2BaCu_8Te_{10}$.

Charge transport measurements on $K_2BaCu_8Te_{10}$ and $Rb_2BaCu_8Te_{10}$ indicated that they are similar to $K_4Cu_8Te_{11}$. The electrical resistivity data for $Rb_2BaCu_8Te_{10}$ are shown in Figure 10. Note that the resistivity near room temperature is quite low and remains more or less flat with falling temperature until ∼150 K before it starts rising at lower temperatures. The potassium analog behaves similarly. This behavior suggests that either these materials are degenerate semiconductors or they possess very small band gaps. To confirm this we performed solid-state diffuse-reflectance spectroscopy over a wide range of frequencies. No optical gap was found for $Rb_2BaCu_8Te_{10}$ in the UV/vis/near-IR region (200−2500 nm) where the material absorbs at all wavelengths. The absorption transition across the band gap was found in the mid-IR region (4000−400 cm^{-1}), occurring at about 0.11 eV, see Figure 11.

Magnetic Susceptibility Studies. Variable-temperature magnetic susceptibility data for $Rb_3Cu_8Te_{10}$ and $Rb_2BaCu_8Te_{10}$ over the temperature range 5−300 K are shown in Figure 12. When plotted as χ_m vs temperature, the data for $Rb_3Cu_8Te_{10}$, above 30 K, show weak temperature independent paramagnetism, while below 30 K, the data follow the Curie−Weiss Law. This behavior is characteristic of metals (Pauli paramagnetism) containing a low concentration of paramagnetic impurities. The magnetic susceptibility measurements of $A_2BaCu_8Te_{10}$ (A = K, Rb) indicate temperature-independent diamagnetism, confirming that this class of materials are electron precise with filled valence bands.

Electronic Structure Studies. Tight binding calculations with an extended-Hückel Hamiltonian have been carried out to investigated the bonding in these materials. Computational

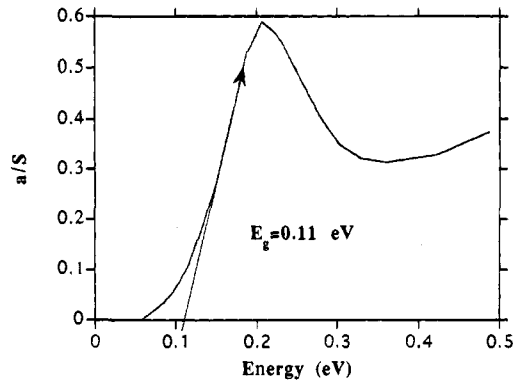

Figure 11. Absorption spectrum calculated from the diffuse reflectance data for $Rb_2BaCu_8Te_{10}$ showing the presence of an electronic transition at ~0.11 eV.

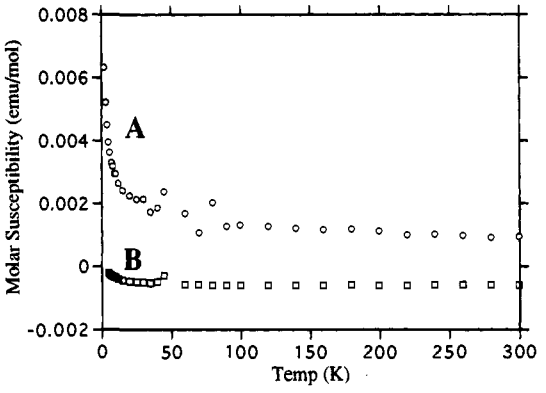

Figure 12. Variable-temperature magnetic susceptibility data for (A) polycrystalline $Cs_3Cu_8Te_{10}$ and (B) $Rb_2BaCu_8Te_{10}$.

details are given in the Experimental Section. A density of states (DOS) plot for a two-dimensional calculation of one layer in $Cu_8Te_{10}^{3-}$, as a model for compounds **2**–**5**, is presented in Figure 13. The Fermi level for this electron count is labeled by ϵ_F in the figure. As mentioned previously, the telluride p levels energetically lie above the copper d atomic orbitals and, therefore, the states around the Fermi level (−10.6 eV) are predominately tellurium in character. This is confirmed by noting the projection of Te, given by the dashed line, in Figure 13. The copper d region lies from ~−13.2 to −15.9 eV, whereas that for tellurium runs from −10.3 to ~−13.2 eV. The introduction of one electron, yielding a $Cu_8Te_{10}^{4-}$ formula unit which is appropriate for compounds **6**–**8**, fills the states just above the Fermi level, creating a band gap. This is in general agreement with the electron counting and charge transport measurements described above.

Compounds **2**–**8** posses three types of coordination environments for tellurium. The Te(4) atoms are monotellurides with a local square pyramidal coordination, **9**. Te(1) and Te(2) represent the shared ditellurides, **10**, and Te(3) are the unshared ones, **11**. Because of the relative ordering for the copper and tellurium atomic orbitals, the copper d atomic orbitals will interact with and destabilize tellurium p in **9**. The copper s

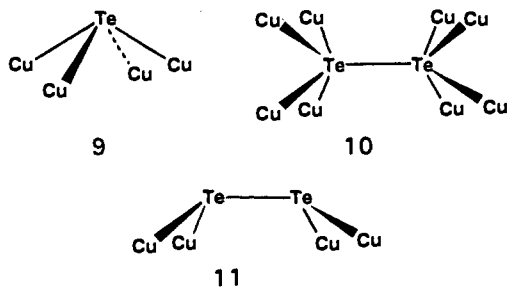

9 10 11

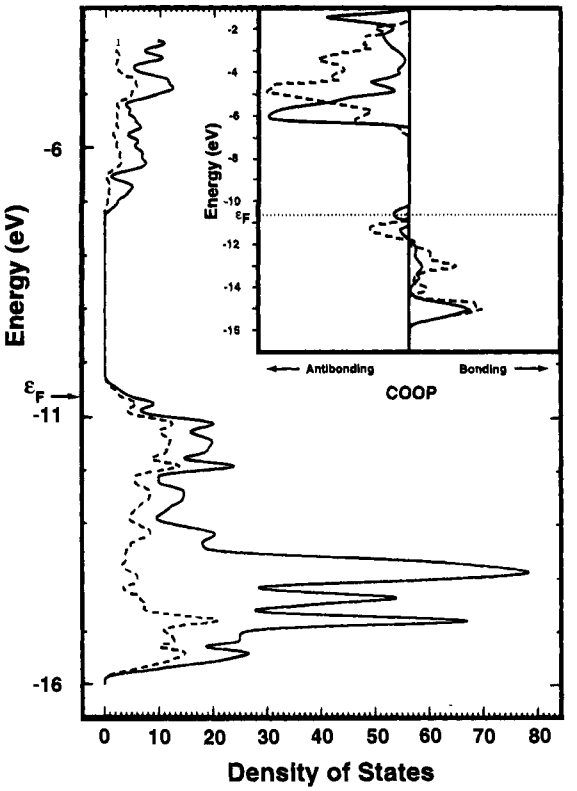

Figure 13. DOS plot for one layer of $Cu_8Te_{10}^{3-}$. The Fermi level is indicated by ϵ_F, and the Te projection is given by the dashed line. The insert at the upper right corner presents the COOP curve for this material. The solid line refers to the Te−Te overlap population for the shared tellurium atoms while the dashed line corresponds to the unshared tellurium atoms. The dotted line indicates the position of the Fermi level.

and p atomic orbitals can mix into the tellurium p states in a bonding fashion. The Te_2^{2-} units are further delocalized by forming σ and π combinations. The highest occupied levels associated with Te_2^{2-} are then the π_g set and the $2\sigma_u^+$ is unoccupied. These orbitals are illustrated by **12**. Copper d

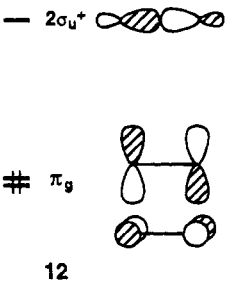

12

along with s and p will again destabilize and stabilize, respectively, the combinations in **12** which are represented by the coordination geometries given by **10** and **11**. The Te−Te π antibonding in π_g will make the Te_2^{2-} states lie higher in energy than the Te^{2-} ones, and thus, they should be concentrated at the Fermi level for $Cu_8Te_{10}^{3-}$. Indeed we find this to be the case when we carry out a calculation on a pentagonal dodecahedral $Cu_8Te_{12}^{4-}$ saturated cluster.[27] With T_h symmetry, the π_g set forms the 12 combinations given in **13**. Here only one member of each degenerate set is shown. For visualization purposes, the copper coefficients are not given; their contributions are small: 25% for a_g and as little as 17% for $2t_u$. The $1t_g$–e_g molecular orbitals lie within a narrow energy interval

(27) The same electronic stucture results in this region when the copper atoms are capped by hydrogens or tellurium atoms to build a local tetrahedral geometry around copper.

13

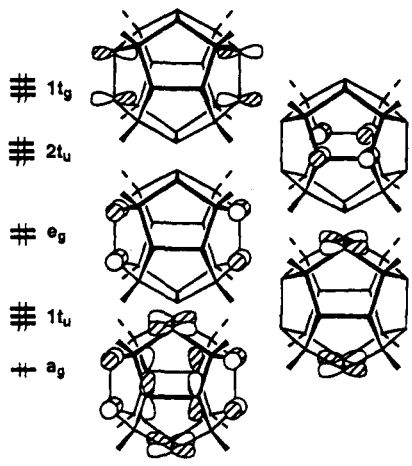

of 0.3 eV, and the $1t_{1u}$ and a_g orbitals are essentially degenerate and only 0.3 eV below the others. When the Cu_8Te_{10} cluster is spread out into the $Cs_3Cu_8Te_{10}$ extended solid, of course, these states become more dispersed; however, examination of the highest bands in the Fermi region show, them to be simply derivatives of those given by **13**. We can pinpoint more generally these states by looking at the crystal orbital overlap population (COOP)[28] curve for Te−Te bonding which is shown in the insert at the upper right side of Figure 13. The solid curve measures the Te−Te overlap population for the shared Te_2^{2-} ligands of type **10**, while the dashed curve is for the unshared ligands **11**. The dotted line marks the Fermi level. As expected, the shared Te_2^{2-} ligand orbitals derived from π_g (**12**) are pushed to slightly higher energies by the copper d orbitals and, thus, predominate at the Fermi level. The unshared Te_2^{2-} components of π_g lie at slightly lower energies, from −10.9 to −11.8 eV. It can be seen from the COOP curve that the Te_2^{2-} π_u bonding analogs are in the region of ∼−12.0 to −14.2 eV. They are extensively delocalized with the copper d manifold.

The lowest unoccupied molecular orbitals of a pentagonal dodecahedral $Cu_8Te_{12}^{4-}$ cluster are derived from the $2\sigma_u^+$ fragment of Te_2^{2-} (**12**). The six combinations are of t_g and t_u symmetry. One member of each set is illustrated in **14**. The

14

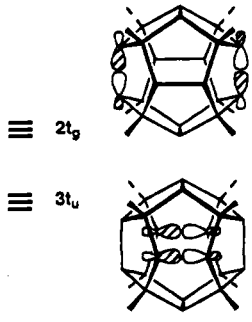

energy difference between the two sets is only 0.2 eV. Copper s and p do mix into $2t_g$ and $3t_u$ in a bonding way, but $2t_g$ and $3t_u$ each still contain 80% Te character. The large antibonding peaks for the COOP curve in Figure 13 which start at −5.9 eV correspond to the delocalized equivalents of **14**. The σ bonding analogs are associated with the two large bonding peaks in the COOP curve centered at −14.9 eV. Here is where there is a problem with the calculations. With the parameter set used for Te, the σ type overlap between two tellurium atoms is modeled to be much too large. The experimental results from the previous section show that $Cu_8Te_{10}^{4-}$ is a narrow band gap semiconductor. The gap between the delocalized states corresponding to **13** and **14** is predicted to be much too large as a consequence of the anomalously large σ overlap (the $2t_g$ and $3t_u$ types of states are put at too high of an energy). We have seen this in other CuTe work[6c] which focused on Te−Te interactions. Therefore, the ∼2.5 eV gap seen for the DOS curve in Figure 13 is greatly overestimated. Nevertheless, the basic features of the electronic structure do follow those derived from a cluster model and ideas based on perturbation theory.

Concluding Remarks

The work reported here represents a significant contribution to the Cu/Te chemistry which is considerably different from that of the Cu/S, Se systems. While the solid-state structures obtained from the alkali polysulfide or polyselenide fluxes are frequently built on long-chained Q_x^{2-} ($x > 3$) ligands, these Cu/Te structures contain only monotellurides and ditellurides. Unlike the lighter polychalcogenides which are generally wide-band-gap semiconductors, the copper tellurides possess high electrical conductivities either due to mixed valency or because of narrow band gaps. The unprecedented pentagonal dodecahedral cage of $Cu_8(Te_2)_6$ is beautifully manifested as a building block with strong affinity for K^+, Rb^+, Cs^+, and Ba^{2+} ions. It is intriguing to conceive this cluster as a structure-directing element in a variety of other solids. One can envision the possibility of building up novel extended structures in one, two, and three dimensions based on this dodecahedral $M_8(Te_2)_6$ cluster by sharing ditelluride edges. Of course, the dodecahedral cluster might be sufficiently stable to be found in discrete molecular form, even though we are not aware of such an example.

Acknowledgment. Financial support from the Office of Naval Research (Contract No. N00014-94-1-0935) is gratefully acknowledged. The X-ray instrumentation used in this work was purchased in part with funds from the National Science Foundation (CHE-8908088). This work made use of the SEM facilities of the Center for Electron Optics at Michigan State University. The work at Houston was supported by the Robert A. Welch Foundation, the Petroleum Research Fund as administered by the American Chemical Society, and the State of Texas through a grant from the Texas Center for Superconductivity at the University of Houston. We thank the National Science Foundation for a generous grant of computing time at the Pittsburgh Supercomputing Center. M.G.K. thanks Alexander Kanatzidis for many fruitful discussions.

Supporting Information Available: Tables of isotropic and anisotropic thermal parameters of all atoms, positional parameters, bond distances and angles, and calculated and observed X-ray powder diffraction patterns (26 pages). This material is contained in many libraries on microfiche, immediately follows this article in the microfilm version of the journal, can be ordered from the ACS, and can be downloaded from the Internet; see any current masthead page for ordering information and Internet access instructions.

JA951728W

(28) Hughbanks, T.; Hoffmann, R. *J. Am. Chem. Soc.* **1983**, *105*, 1150.